International Journal of Advances in Engineering and Management (IJAEM)
Volume 4, Issue 6 June 2022, pp: 17-39 www.ijaem.net ISSN: 2395-5252

Comparative Analysis of the Propulsion System for a Tug Boat for Optimal Performance Using Aluminium or Steel Material

Nitonye S, Olla O, Ijala O, Okparajiaku O. S., Joe-Jim S A, Kpegasin P Z, Amadigwe S C
Rivers State University, Port Harcourt, Nigeria

Submitted: 25-05-2022 Revised: 01-06-2022 Accepted: 05-06-2022

ABSTRACT: The propulsion system consists of three parts: the main engine, the transmission shaft and the propeller. This project designed the propulsion system of a tug boat using a computer aided design software. Analysis was carried out on the piston material of the Main Engine, the materials considered are aluminium, Steel and Grey cast iron. These analyses were doneto determine the total deformation condition of each material at a pressure of 6.289bar at the top of the piston and average cycle pressure of 80bar. It was observed that steel is a better material for the piston in terms of both deformation and stress while aluminium is not a good material for piston choice. Graphs were used to explain the analysis. In the case of the shafting line, discussion were made on how the reduction gear gives a standard required thrust for the shafting drive line to move the propeller at the efficient torque and revolution and the shafting system, analysis were carried out on the materials used for the shafting system which are aluminium and stainless steel, it was observed that deformation on aluminium is higher than that on the stainless steel at 1800N but the stress distribution on aluminium is lesser to that of the stainless steel. In the case of the propeller analysis were carried out on the pressure and around the propeller with the rotation velocity from 200rpm-400rpm. Gradient are used to show the pressure distribution, fluid behaviour around the propeller and also indicates the maximum and minimum pressure on the propeller. It was observed that at 350rpm the pressure distribution is minimal to others velocity rotation and the thrust force at 400rpm gives the maximum thrust force and steady time line. In conclusion Aluminium is not a better material for the design and construction of marine propulsion system in a tug boat, Steel proves to withstand more pressure in the Engine other than that of the aluminium

KEYWORDS: Diesel Engine, Propeller, shaft Aluminium, steel, thrust force, solid work software 2018.

I. INTRODUCTION

The technological advancement and development in the use of software have made several analysis very easy and increased quantities of production. This work will explore the influence of each component in the propulsion system of a tug boat by using software to analyse the impact at maximum load using the steel material or the aluminium. Propulsion is the action or process of pushing or pulling to drive an object forward. The term is derived from two Latin words: pro, meaning before or forward; and pellere, meaning to drive [1]. A propulsion system consists of a source of mechanical power, and a propulsor. Technology system uses an engine or motor as the power source, and wheels and axles, propellers, or a propulsive nozzle to generate the force. Propulsion in vessels is needed not only to go ahead against natural forces, but to decelerate and stop, and even to keep position at the surface or under water. A propulsion system consists of three parts: an energy, an engine that transforms it to a mechanical form, and the propulsor or thruster [2]. The aim of this study is to do a comparative analysis of the propulsion system of a tugboat for optimum performance using steel or the aluminium materials considering the engine system, the shaft system and the propeller system extensively in analysis and to analyse the effect of

International Journal of Advances in Engineering and Management (IJAEM)
Volume 4, Issue 6 June 2022, pp: 17-39 www.ijaem.net ISSN: 2395-5252

power and heat on the piston, propeller shaft using aluminium and steel using a computer software "Ansys" to compare the numerical result of the design analysis [3]

Diesel Engine

The diesel engine was invented by **Rudolf Diesel**, who was a German inventor and mechanical engineer, because of the heavier, more robust construction requirements of the diesel engine it has never been widely used in the aviation industry but is ideal for other applications, particularly trains, boats and ships. In high-speed engines, diesel fuel injection commonly occurs at about 20° before top dead centre [4], [5], [6]. Fuel is injected at high pressure, in atomized form and with a very high-speed reaching 250m/s. The injected fuel combustion occurs in 3 stages. Stage one consists of physical lag, where injected fuel mixes and vaporizes into the hot air of combustion chamber. This stage is called "ignition delay" and defined as "the time laps between the fuel injection and the first rise in pressure due to exothermic reaction of combustion of fuel" [7], [8], [9]. In stage two, some of the vaporized fuel burns in an explosion like combustion causing a sharp and quick increase in pressure inside the combustion chamber; this is commonly known as the premature combustion. This explosion like combustion separates between fuel and air, allowing them to diffuse and burn smoothly in the third stage of combustion, namely the diffusion stage [10], [11]. The time required by various stages of combustion affects the efficiency and emissions of diesel engines, and therefore plays an important role in optimization. Generally speaking, a long physical lag results in a strong pre-combustion causing impaired starting ability, while a short ignition lag shifts the combustion to the less efficient diffusion stage increasing particle matter emission (black smoke), specially at high loads [12]. Ignition lag as such is mainly a function of fuel quality commonly called cetane number.

Constructional Features of IC Engine

The cylinder of an internal combustion (IC) engine constitutes the basic and supporting portion of the engine power unit. Its major function is to provide space in which the piston can operate to draw in the fuel mixture or air (depending upon spark ignition or compression ignition), compress it, allow it to expand and thus generate power. Figure 1 shows the features of the IC engine

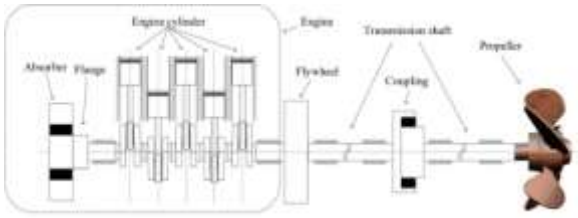

Figure 1: The features of IC Engine

The cylinder is usually made of high-grade cast iron. In some cases, to give greater strength and wear resistance with less weight, chromium, nickel and molybdenum are added to the cast iron. The piston of an engine is the first part to begin movement and to transmit power to the crankshaft as a result of the pressure and energy generated by the combustion of the fuel. The piston is closed at one end and open on the other end to permit direct attachment of the connecting rod and its free action. The materials used for pistons are grey cast iron, cast steel and aluminium alloy. However, the modern trend is to use only aluminium alloy pistons in the tractor engine.

The Propeller

A **propeller** is a device with a rotating hub and radiating blades that are set at a pitch to form a helical spiral, that, when rotated, exerts linear thrust upon a working fluid, such as water or air. Propellers are used to pump fluid through a pipe or duct, or to create thrust to propel a boat through water or an aircraft through air. The blades are specially shaped so that their rotational motion through the fluid causes a pressure difference between the two surfaces of the blade by Bernoulli's principle which exerts force on the fluid. Most marine propellers are **screw propellers** with helical blades rotating on a propellershaft with an approximately horizontal axis [13], [14].

There are different types of propulsion system for marine operation. Diesel electric propulsion system is one of the propulsions that has configuration that is fitted with the bow and aft thrusters, and is often mounted with one up to eight azimuth thrusters. The bow and aft thrusters are electrically driven All though the impacts of these ships on the whole maritime industry is most times been neglected, but their value is mostly felt in manoeuvring during bad weather conditions and during vessel breakdown etc. The effectiveness of a tug boat is characterized by its ability to tow and man oeuvre easily, which is a major concern in the marine industry. Most important factor is propulsive design is the interaction between the propeller and the nozzle with the hull [15], [16]

International Journal of Advances in Engineering and Management (IJAEM)
Volume 4, Issue 6 June 2022, pp: 17-39 www.ijaem.net ISSN: 2395-5252

Worldwide, tugs are most recognized for their work in assisting large ships to and from their berths and for their role as salvage vessels when ships get into trouble. Typically, tugs are categorized according to the type of work they do, and then by the configuration or type of propulsion system used. The following are the most common descriptions used for the latter, as well as a few other commonly used terms in the industry [17].

Tugboats have been an indispensable part of maritime transportation for nearly 200 years. They man oeuvre larger watercraft in tight areas, and tow unpowered vessels from port to port. Tugs were invented in the 1810s, shortly after steam-power was successfully applied to watercraft. During the 1800s on the Hudson River and Lake Champlain, old stripped-down side-wheelers and propeller-driven towboats were used to move ever-increasing numbers of watercraft, especially canal boats [18], [19], [20].

Tug boats are small but very powerful vessel used in towing or tugging bigger vessels that cannot move by themselves or are not self-propelled like some barges. The strength of a tug boat and its ability to maneuver effectively depends solely on the propulsion system installed, starting from the main engines to the gear box, the shafting system and the propellers. Tugboat engines produces power ranging from 500 - 2500 KW (680 - 3400 HP). Since tugboats are designed to be highly maneuverable, different kinds of propulsion systems have been developed [20]

Ganesh and his colleague modelled and analyzed a propeller blade of a torpedo for its strength. CATIA software was used for developing the blade model, while model analysis and static structural analysis were carried out for both Aluminum and CFRP on ANSYS. By considering the design of the propeller blade on the basis of a cantilever beam, the hub was taken to be the fixed end where there was no deformation. On carrying out model analysis for both aluminum and composite propellers, they found that the maximum displacement for composite propeller is less than the Aluminum propeller [21].

Mohammed researched in 2013 with his colleague to carried out the dynamic analysis of Propellers of different materials, namely aluminium, CFRP and GFRP. The solid model of propeller was developed using CATIA V5 R17 and using HYPER MESH, a tetrahedral mesh was generated for said model. They carried out static, Eigen and frequency responses analyses of both aluminum and the composite propeller on ANSYS. They also calculated inter- laminar shear stresses for composite propeller by varying the number of layers and found that the percentage variation was about 3.147% [22]

Seetharama et al (2012) presented a methodology to design a propeller with a metal and composite material, and perform stress analysis in order to evaluate its effectiveness using ANSYS software. Proposed methodology showed substantial improvements in metal propellers. Analytical methods were first carried out to find out stresses in a blade section and then, the mean deflection; normal stress and shear stress were found for both metallic and composite propeller by using ANSYS. From their results of stress analysis, the stresses of composite propeller were obtained are within the allowable stress limit [23].

Palle & Lanka (2017) worked on the structural analysis of a CFRP (carbon fibre reinforced plastic) propeller blade which was a replacement to the Aluminum propeller blade. They subjected the propeller to external hydrostatic pressure on either side of the blade. From the output of their static analysis and dynamic analyses of the marine propeller, they concluded that the propeller is assumed as a cantilever beam and by varying the material for propeller blade from CFRP to GFRP, the Von- Mises stress is reduced to a percentage of 31.4% [24].

Abhijeet & Kachare (2012) explained how propeller parameters were based on number of blades, sizing, power and rpm, speed of the ship. He modelled a propeller on CATIA, after which a mesh was generated using HYPERMESH. Static and harmonic analyses were both performed on ANSYS for Aluminum and Composite material-based propellers. He found that the deflection of Composite propeller was much lower than the Aluminum propeller, indicating its stiffness. Also, from the Harmonic Analysis, he found out that the operating range of Composite propellers were much higher than the Aluminum propellers. In February 1800, Edward Shorter of London proposed using a similar propeller attached to a rod angled down temporarily deployed from the deck above the waterline and thus requiring no water seal, and intended only to assist becalmed sailing vessels. He tested it on the transport ship Doncaster in Gibraltar and at Malta, achieving a speed of 1.5 mph (2.4 km/h) [25], [26], [27].

II MATERIALS AND METHODS

The main objective of this research is to analyse the propulsion system of a tug boat using a

International Journal of Advances in Engineering and Management (IJAEM)
Volume 4, Issue 6 June 2022, pp: 17-39 www.ijaem.net ISSN: 2395-5252

computer aided design software, the features to be designed include: Diesel engine, Drive shaft and Propeller. For the **Diesel Engine** the practical maximum output of a marine diesel engine may be said to have been reached when one or more of the following factors operate: The maximum percentage of fuel possible is being burned effectively in the cylinder volume available, the stresses in the component parts of the engine generally, for mechanical and thermal conditions prevailing, have attained the highest safe level for continuous working and the mean piston speed and thus revolutions per minute (rpm) cannot safely be increased.

Engine Design

In the process of designing any engine the brake horsepower and rpm are related by the following formula

$$BHP = \frac{P_e \cdot V_s \cdot n \cdot Z}{C} \quad (1)$$

Mean effective pressure (P_e) can be calculated from indicated pressure P_i, by assuming mechanical efficiency η_m (around 0.85).

As shown in the previous equation, if P_e is determined, the engine bore, stroke and number of cylinders can be calculated. Before the widespread use of computers in the process of engine design, the only way to calculate P_e was from using equations derived from the (p-v) curve. Nowadays, computers make it a lot easier for designers, and the equations that consumed days and days of calculations are now solved in few seconds [28]

Cylinder Liners

The following formula could be used to calculate maximum liner thickness taking into account mechanical stresses only.

$$\tau_{Max} = \frac{D}{2} \times \left[\sqrt{\frac{\sigma + P_{max}}{\sigma - P_{max}}}\right] + \tau_a \quad (2)$$

Table 1 shows the design parameters for the cylinder

Table1: Design parameters

Item	Value	Unit
Cooling losses	0.25	-
Exhaust losses	0.3529	-
Brake thermal efficiency	0.3375	-
Bsfc	187.2	gm/kwh
Bore	38.01	cm
Stroke	47.51	cm
Bmep	26.7	bar
Maxcylinder pressure	164.6	bar

Where:

t_{max} is the maximum liner thickness, mms,
D is the Cylinder bore, mms,
σ is the allowable stress, bar,
P_{max} is the max cylinder gas pressure, bar, and
t_a is the allowance for reboring or regrinding, mms.

Solving for t_{max} = 37.334 mm

Piston Design

As a general practice, calculations are made for the following parts of the piston: skirt (or body), crown, piston pins and piston rings.Assuming that the piston crown is subjected to a uniformly distributed load of the maximum gas pressure Pmax, Faust equation can be used to calculate the stresses resulting from the pressure of the combustion gases on the piston crown, the thermal stresses are included in the constant of the equation as a factor of the mechanical load.

$$\frac{\sigma_{max}}{P_{max}} = C\left(\frac{r}{h}\right)^2 \quad (3)$$

Where:

"C" is the 1.25,
"h" is the crown thickness, cms,
r is the piston radius, cms,
P_{max} is the maximum gas pressure, bar, and
σ_{max} is the high allowable stress for steel.

Solving equation 3, h = 7.037 cm

Piston Rings

Piston rings are made from special cast iron having high elasticity.

Let "b" be the length of the ring which presses the cylinder, and a is the breadth

$$b = D\sqrt{\frac{3P}{f_b}} \quad (4)$$

$$a = \frac{D}{25} \quad (5)$$

Where:

P is the pressing force (ring on cylinder), and

International Journal of Advances in Engineering and Management (IJAEM)
Volume 4, Issue 6 June 2022, pp: 17-39 www.ijaem.net ISSN: 2395-5252

f_b is the high allowable stress of ring material (centrifugal cast iron).
Solving (4 and 5), b=1.61cm, a=1.52 cm

The Shaft

A shaft is a mechanical component for transmitting torque and rotation, usually used to connect other components of a drive train that cannot be connected directly because of distance or the need to allow for relative movement between them. As torque carriers, shafts are subject to torsion and shear stress, equivalent to the difference between the input torque and the load. They must therefore be strong enough to bear the stress, whilst avoiding too much additional weight as that would in turn increase their inertia [29], [30].

ANSYS is commonly used extensively in structural analysis. ANSYS consists of three main phases: pre-processing, conducting or importing of the solid model system that is to be analysed, solid meshing design in finite elements, implementation of boundary conditions and loads limit, processing, numeric solving of the characteristic equations of the system and getting the solution. Post-processing, viewing the results to analyse system reaction and identification of areas with critical applications

In this project we considered a drive shaft used in a tug boat to be analysed structurally. the result is aimed at knowing the best material and thickness suitable for a drive shaft used on a tug boat to reduce the rate at which tug boats visit the dockyard due to shaft failure. We will be considering 3 materials for this simulation; Stainless steel, Aluminium alloy and Grey cast iron

Modelling and Analysis Procedure

Using SolidWorks, we first make the part (shaft) that we are going to use for the analysis and save IGES format. Then we browse the part in ANSYS Workbench. In ANSYS Workbench, we select 'Static Structural Analysis' as our work. Then, we Import the materials amongst available engineering materials. In the Design modular, first of all we assign the materials to the part respectively. Then we set the co-ordinate system according to our requirement.For the next step, we apply the necessary boundary conditions, we apply 'cylindrical support' to the cylindrical extension of the shaft, keep the tangential component 'free' so that the shaft can rotate about its axis of rotation and apply angular rotation to the pulley of magnitude '1800 rev/min'.Table 2 shows the material property of stainless steel and aluminium alloy

Table 2: Material Property of stainless steel and aluminium alloy

	Stainless Steel		Aluminum Alloy	
Property	value	Unit	Value	Unit
Density	7750	Kg/m^3	2770	Kg/m^3
Coeffof thermal expansion	1.7E-05	K	2.3E-05	K
Young's Modulus	1.93E+11	Pa	7.1E+10	Pa
Poisson's Ratio	0.31		0.33	
Bulk Modulus	1.693E+11	Pa	6.9608E+10	Pa
Shear Modulus	7.3664E+10	Pa	2.6692E+10	Pa
Tensile yield strength	2.07E+08	Pa	2.8E+08	Pa
Tensile ultimate strength	5.86E+08	Pa	3.1E+08	Pa

Geometric Modelling

The modelling of marine propeller was done using the computer aided design software Solid works 2018.The following were the steps involved in developing the Solid works models of the propellers; a horizontal line of was drawn, and from the starting point of the same line, a vertical line was drawn. These lines represent the length and the radius of the Hub of the Propeller respectively. From the end of the radius line, a horizontal line was

International Journal of Advances in Engineering and Management (IJAEM)
Volume 4, Issue 6 June 2022, pp: 17-39 www.ijaem.net ISSN: 2395-5252

drawn. From this point, a spline connected this line to the line representing the length of the propeller. This was curved in such a way that it was concave to the centre of the surface. 0This drawing was revolved about the length, thus completing the hub

A rectangle was drawn at the centre of the propeller, perpendicular to its axis . Another rectangle of the same dimensions was drawn above the central axis , angled 74̊ to the horizontal. This is the radius of the propeller blade. The rectangle at the central axis is lofted to the rectangle above , and this forms the initial blade . Upon providing necessary fillets at the blade edges , it is skewed by 20˚ when viewed from the front. Also, a hole is cut at the rear end of the hub, which is where the shaft would be assembled. The propeller blade is ready as shown in figures 2 and 3. Depending on the number of blades, a circular pattern of 5 blades, spaced equally around the circumference of the hub.

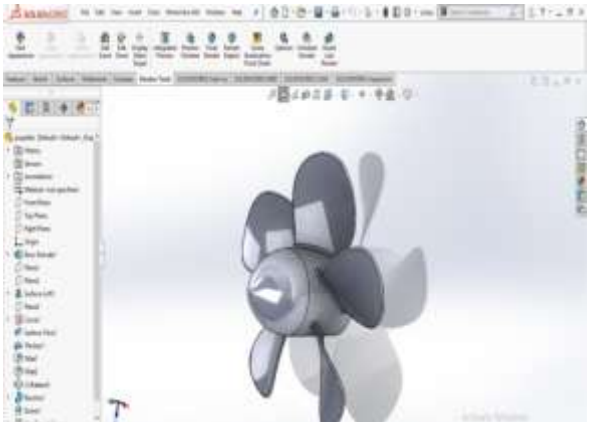

Figure 2: 3D model of marine propeller

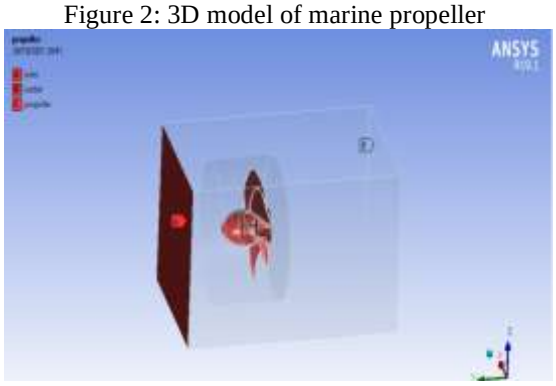

Figure 3: boundary condition setup

The continuum was chosen as fluid and the properties of water were assigned to it. A moving reference frame is assigned to fluid with a rotational velocity (300 rpm and 350 rpm). The wall forming the propeller blade and hub were assigned a relative rotational velocity of zero with respect to adjacent cell zone. A uniform velocity 0.514m/sec was prescribed at inlet. At outlet outflow boundary condition was set. The far boundary (far field) was taken as inviscid wall and assigned an absolute rotational velocity of zero. Table 3 shows the simulation conditions for the propeller

Table 3: Simulation conditions

Case	Propeller Speed (rpm)
1	200
2	250
3	300
4	350
5	400

International Journal of Advances in Engineering and Management (IJAEM)
Volume 4, Issue 6 June 2022, pp: 17-39 www.ijaem.net ISSN: 2395-5252

III RESULT AND DISCUSSION

Simulation results for the Piston

The applications of various types of pistons are: Trunk pistons are used in marine diesel engines, Crosshead pistons are used in steam locomotives, Slipper pistons are used in petrol engines like in Formula1 and Moto GP where high performance is required and Deflector pistons are used where gas flow in cylinder must be carefully directed in order to provide efficient scavenging. In this present work three materials were selected for carrying out analysis, they are Aluminium, Grey Cast iron and Structural steel. The properties of the selected materials are as shown in Table 4 while Tables 5 to 7 shows the extracted date for cases 1 to 3 from the ANSYS Workbench

Table4: Material properties of aluminium, grey cast iron and structural steel

Properties	Aluminum Alloy	Grey Cast Iron	Structural Steel	Unit
Density	2770	7200	7850	Kg/m^3
Tensile Yield Strength	2.8E+08	0	2.5E+08	Pa
Tensile Ultimate Strength	3.1E+08	2.4E+08	4.6E+08	Pa
Young's Modulus	7.1E+10	1.1E+11	2E+11	Pa
Poisson's Ratio	0.33	0.28	0.3	
Bulk Modulus	6.9608E+10	8.3333E+10	1.6667E+11	Pa
Coefficient of thermal expansion	2.3E-05	1.1E-05	1.2E-05	^oC
Shear Modulus		4.2969E+10	7.6923E+10	Pa
Compressive Yield Strength	2.8E+08	0	2.5E+08	Pa
Compressive Ultimate Strength	0	8.2E+08	0	Pa

Table5: Extracted data for case 1 from ANSYS.

Definition				
Type	Total Deformation	Equivalent (von-Mises) Stress	Minimum Principal Stress	Maximum Shear Elastic Strain
Results				
Minimum	0. m	0.47425 Pa	-3.3608e+006 Pa	3.5554e-012 m/m
Maximum	2.7259e-007 m	2.9199e+006 Pa	64251 Pa	2.1295e-005 m/m
Average	2.9023e-008 m	3.5267e+005 Pa	-2.8908e+005 Pa	2.6159e-006 m/m

Table6: Extracted data for case 2 from ANSYS.

Type	Total Deformation	Equivalent (von-Mises) Stress	Minimum Principal Stress	Maximum Shear Elastic Strain
Minimum	0. m	1.8697 Pa	-7.5576e+006 Pa	4.0438e-011 m/m
Maximum	1.2207e-006 m	6.4108e+006 Pa	7.862e+005 Pa	1.3562e-004 m/m
Average	2.7581e-007 m	5.8273e+005 Pa	-5.6888e+005 Pa	1.2354e-005 m/m

Table7: Extracted data for case 3 from ANSYS

Type	Total Deformation	Equivalent (von-Mises) Stress	Minimum Principal Stress	Maximum Shear Elastic Strain
Minimum	0. m	0.37882 Pa	-2.8705e+006 Pa	5.0879e-012 m/m
Maximum	4.8716e-007 m	2.8229e+006 Pa	-0.25038 Pa	3.7523e-005 m/m
Average	5.1565e-008 m	3.5086e+005 Pa	-2.8137e+005	4.6561e-006 m/m

International Journal of Advances in Engineering and Management (IJAEM)
Volume 4, Issue 6 June 2022, pp: 17-39 www.ijaem.net ISSN: 2395-5252

Pa

Piston Analysis (Meshing)

The component drawn in Solid Works is imported to ANSYS through its format and then meshing is done for the part. For meshing fine mesh is selected. Figure 4 and 5 shows the modelling and meshing of the piston in ANSYS respectively.

Figure 4: The modelled piston

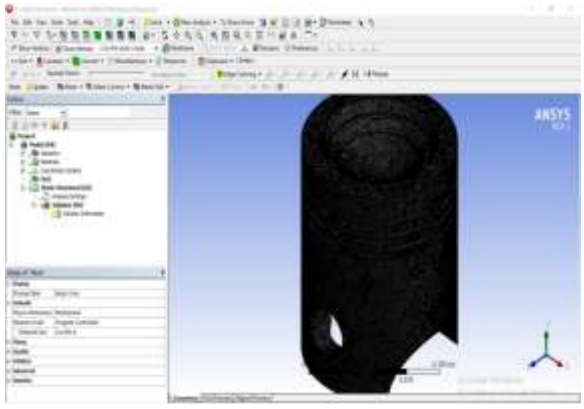

Figure 5: Meshed Piston Model.

A pressure of 6.289 bar is applied at the top of the piston head restraining the piston pin and the average cycle pressure is 80 bar for the full load condition which is taken from the open literature will be applied on the piston head. One by one the material was applied on the piston and then the analysis results are shown below. Static analysis was carried out and results are tabulated. Total deformation and vonmises stress are calculated and found out that which materials suits for the assumed conditions.

For reasons of this project the simulation will be divided into 3 cases, each case will represent a different material specification. Case 1: Structural Steel, Case 2: Aluminium and Case 3: Grey cast iron as shown in figures 6 to 11 respectively.

Case 1 shows the structural analysis of the steel material, the total deformation is calculated based on pressure distribution and average cycle pressure applied on piston head.

International Journal of Advances in Engineering and Management (IJAEM)
Volume 4, Issue 6 June 2022, pp: 17-39 www.ijaem.net ISSN: 2395-5252

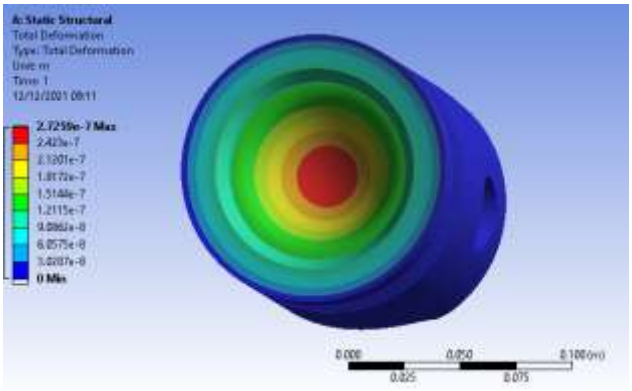

Figure 6: Total Deformation

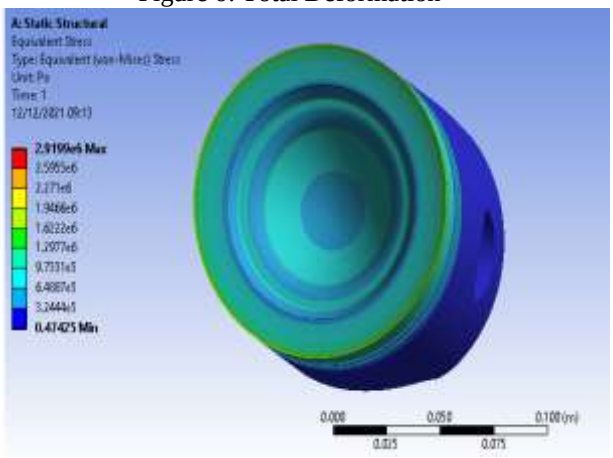

Figure 7: Equivalent stress

Case 2 shows the structural analysis of the aluminium alloy, the total deformation is calculated based on pressure distribution and average cycle pressure applied on piston head.

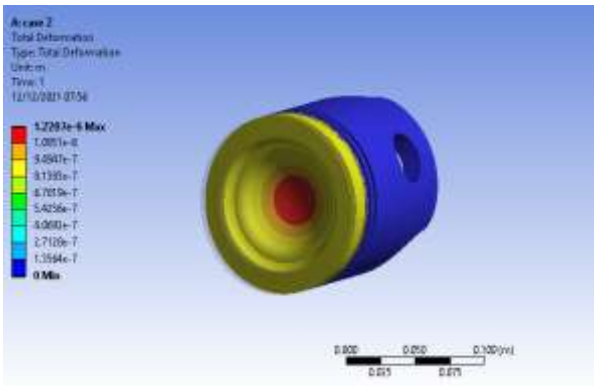

Figure 8: Total Deformation

International Journal of Advances in Engineering and Management (IJAEM)
Volume 4, Issue 6 June 2022, pp: 17-39 www.ijaem.net ISSN: 2395-5252

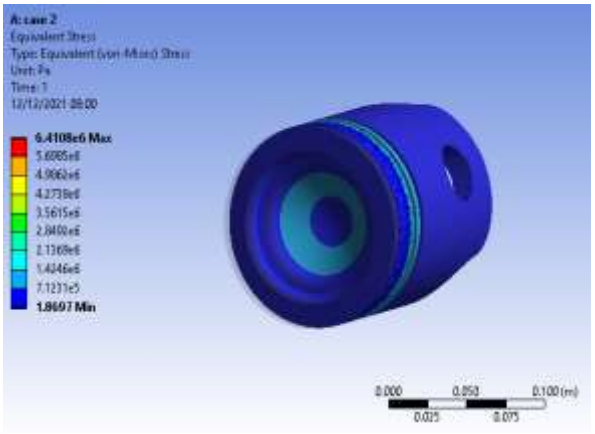

Figure 9:Equivalent stress

Case 3shows the structural analysis of theGrey Cast Iron, the total deformation was calculated based on pressure distribution and average cycle pressure applied on piston head.

Figures 12 to 15 shows the total deformation, equivalentstress, minimum principal stress and maximum shear elastic strain for cases 1-3. The figures are structured to illustrate the varying effect of the force on the diesel engine cylinder with different material applied.

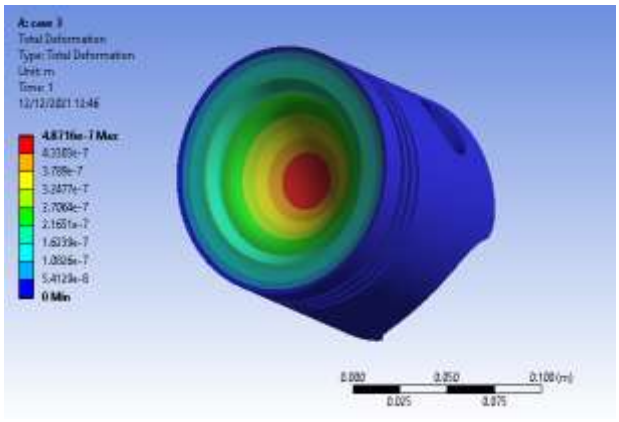

Figure 10: Total deformation contour

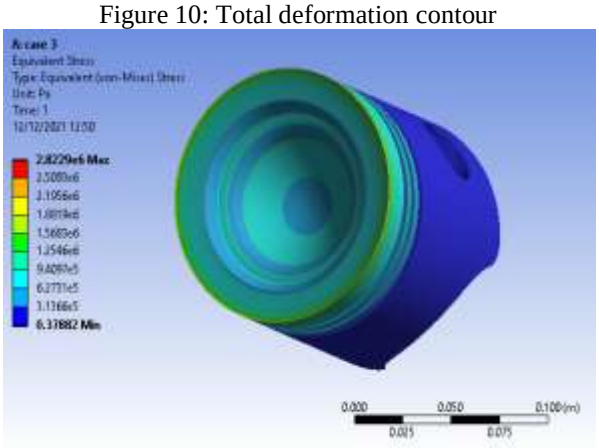

Figure 11: Equivalent stress

International Journal of Advances in Engineering and Management (IJAEM)
Volume 4, Issue 6 June 2022, pp: 17-39 www.ijaem.net ISSN: 2395-5252

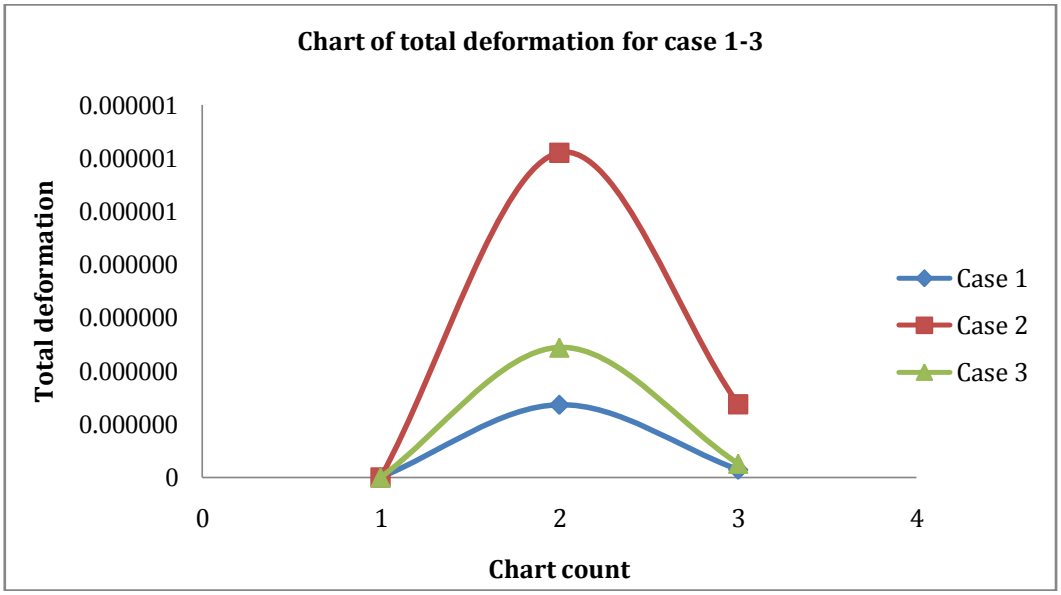

Figure 12: Chart of total deformation

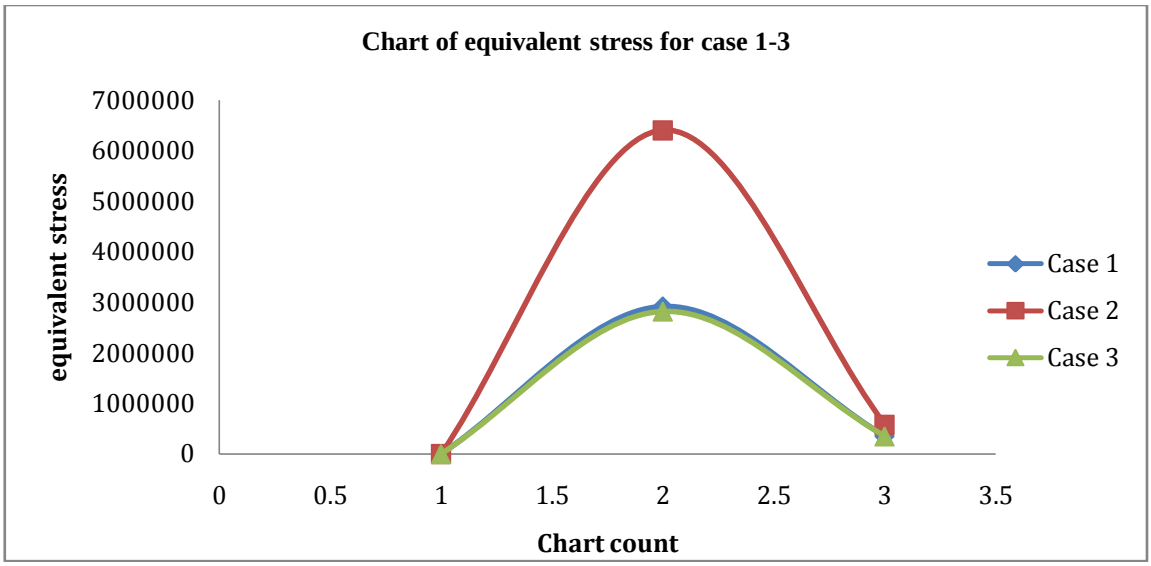

Figure 13: Chart of equivalent (Von Mises) stress

International Journal of Advances in Engineering and Management (IJAEM)
Volume 4, Issue 6 June 2022, pp: 17-39 www.ijaem.net ISSN: 2395-5252

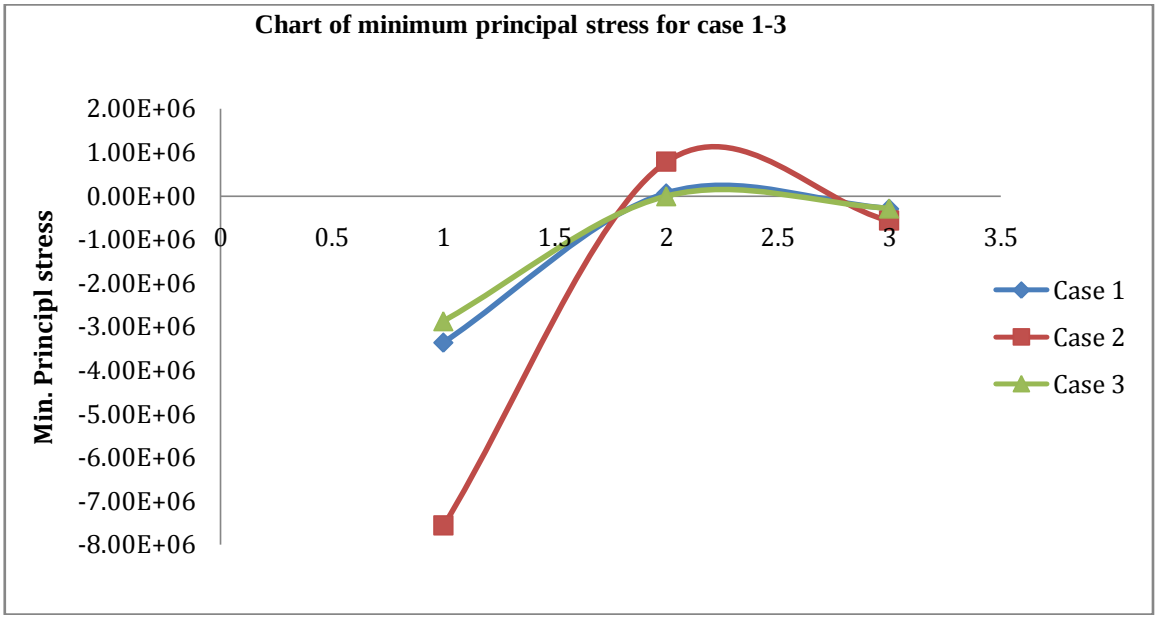

Figure 14: Chart of minimum principal stress

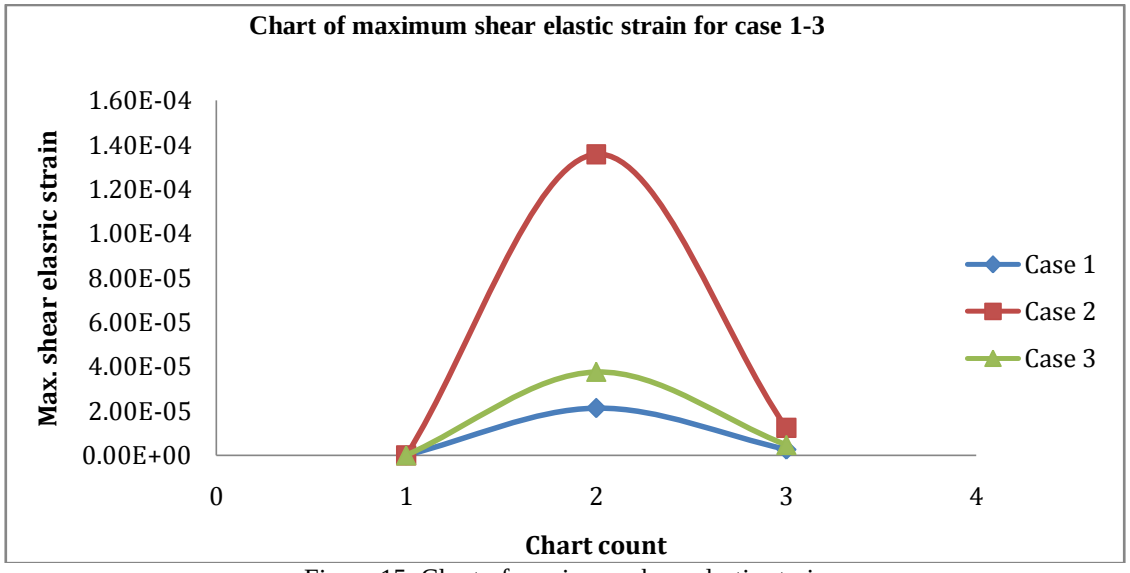

Figure 15: Chart of maximum shear elastic strain

Data Presentation and Analysis

In Table 8, we observe that there was a total of two hundred and ninety-nine boat-visits made to the dockyard. Out of this number, forty-nine represented visits made for maintenance of shaft and gearbox while the remaining counts represented that made for purpose of carrying out repairs following the component's failure. The latter can be interpreted as shaft/gearbox system's failure frequency. Considering the study period, the relatively low frequency of shipvisits to the dockyard for maintenance purposes observed in Table 8, suggests that regular boat maintenance schedule was not adhered to by the skippers. Based on these statistics, the failure or hazard rates and survival probabilities were calculated and plotted to obtain clearer insights into the data set [31], [32], [33], [34]

Table 9 shows the distribution of event times (mean values) when shaft or gearbox (or both) component failed. Based on the table, we find that average time to component failure was 8.33, 5.23 and 5.21 months for tug, supply and crew boats respectively. The zero values represent censored observation denoting situations when there was no failure observed for the propulsion components and the consideration of pollution of the environment from the ship [35]

International Journal of Advances in Engineering and Management (IJAEM)
Volume 4, Issue 6 June 2022, pp: 17-39 www.ijaem.net ISSN: 2395-5252

Table8. Frequency of ship visits to the dockyard and purpose. [32]

Purpose of Visit	Type Of vessel			
	Tug	Supply	Crew	Total
Shaft Failure	17	89	35	141
Gear Box Failure	7	52	14	73
Shaft/gearbox failure	5	21	10	36
Maintenance	5	32	12	49
Total	34	194	71	299

Table9: Average time to event (shaft/gearbox failure or censored)[32]

Boat Type	**Time (Month)**		
	Status	No. of Boats	Mean
Tug	0	5	5.34
	1	29	8.326
Supply	0	32	5.126
	1	162	5.229
Crew	0	12	4.798
	1	59	5.205

Simulation results for the shaft

After running the model, we obtain important information about the stress regions on the shaft. The results of the simulation are presented below:

i. Aluminium Drive Shaft

The figure 16 shows the deformation rate of the drive shaft at the moment of 1800 Nm. With a maximum deformation of 7.688e-004m and minimum deformation rate is 0mm.

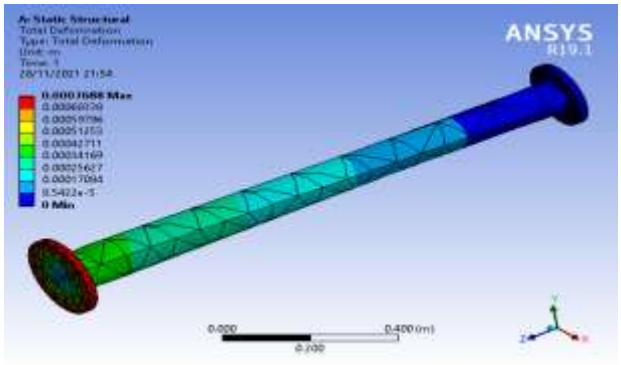

Figure 16: Total deformation on Al alloy shaft

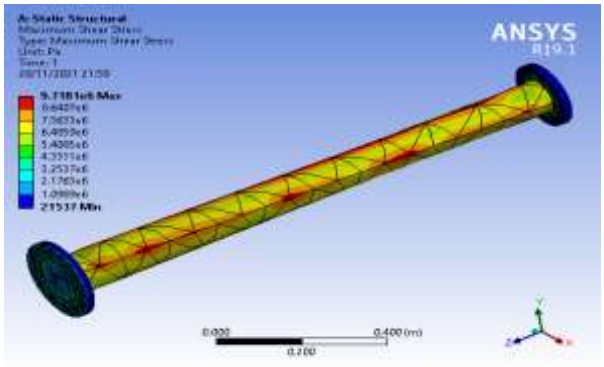

Figure 17: Stress distribution of Al drive shaft

The figure 17 gives the stress distribution of the aluminium drive shaft at 1800 Nm torque applied to it. It shows the maximum stress rate as 9.7181e+006 pa and the minimum stress rate at 21537 pa. And the average stress occurred in the shaft is 2.2325e+006pa.

International Journal of Advances in Engineering and Management (IJAEM)
Volume 4, Issue 6 June 2022, pp: 17-39 www.ijaem.net ISSN: 2395-5252

ii. Stainless Steel Drive shaft

The figure 18 shows the deformation rate of the drive shaft at the moment of 1800 Nm. With a maximum deformation of 2.7869e-004 m and minimum deformation rate is 0mm.

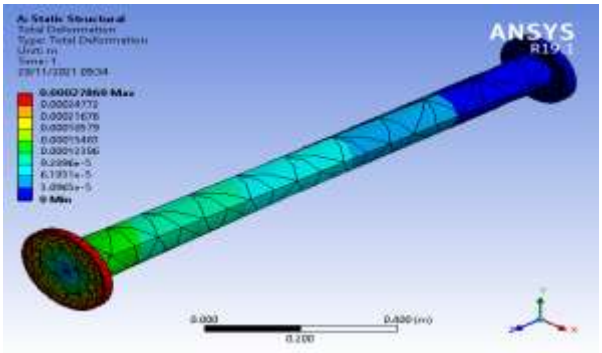

]Figure 18: Total deformation on stainless steel shaft

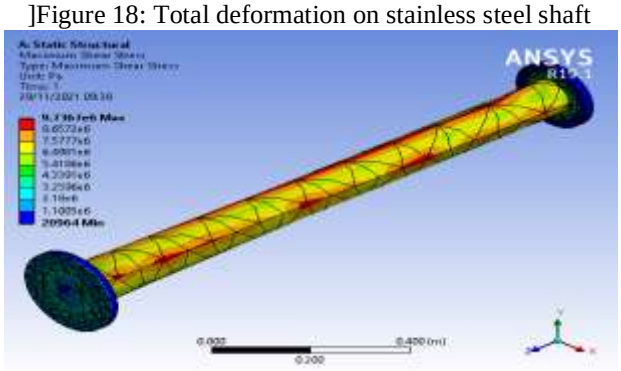

Figure 19: stress distribution of stainlesssteel drive shaft

The figure 19 gives the stress distribution of the stainless-steel drive shaft at 1800 Nm torque applied. It shows the maximum stress rate as 9.7367e+006pa and the minimum stress rate at 20964pa. But the stress occurred in the shaft is 2.2333e+006pa which shows it is safe to use. Table 10 and 11 show the variation between the effect of working load on the aluminium shaft compared to the structural steel shaft while figure 20 illustrates the directional deformation the drive shaft of two distinct materials aluminium and structural steel, showing its maximum, minimum and average directional deformation on both materials. Figure 21 shows the maximum shear stress the drive shaft of two distinct materials aluminium and structural steel, showing its maximum, minimum and average shear stress on both materials. Figure 23shows that there is a total deformation for aluminium of a drive shaft at peak point of 2,7.69E-0.4 and at peak point 2,2.79E-0.4. The structural steel of a drive shaft undergoes total deformation. Figure 24 shows the equivalent stress for both aluminium drive shaft and structural steel drive shaft at the same peak point of 2,1.68E+07 and 2,1.69E+07

Table 10: Stress distribution data for Aluminiumdrive shaft

Object Name	Directional Deformation	Maximum Shear Stress	Maximum Shear Elastic Strain	Total Deformation	Equivalent Stress
Results					
Minimum	-7.655e-004 m	21537 Pa	8.069e-007 m/m	0. m	39301 Pa
Maximum	7.5197e-004 m	9.7181e+006 Pa	3.6408e-004 m/m	7.688e-004 m	1.6832e+007 Pa
Average	-7.203e-006 m	2.2325e+006 Pa	8.3638e-005 m/m	2.8517e-004 m	3.8918e+006 Pa

International Journal of Advances in Engineering and Management (IJAEM)
Volume 4, Issue 6 June 2022, pp: 17-39 www.ijaem.net ISSN: 2395-5252

Table 11: Stress Distribution data for Structural steel Shaft

Object Name	Directional Deformation	Maximum Shear Stress	Maximum Shear Elastic Strain	Total Deformation	Equivalent Stress
Results					
Minimum	-2.7773e-004 m	20964 Pa	2.8459e-007 m/m	0. m	37787 Pa
Maximum	2.7266e-004 m	9.7367e+006 Pa	1.3218e-004 m/m	2.7869e-004 m	1.6865e+007 Pa
Average	-2.6554e-006 m	2.2333e+006 Pa	3.0318e-005 m/m	1.0343e-004 m	3.8942e+006 Pa

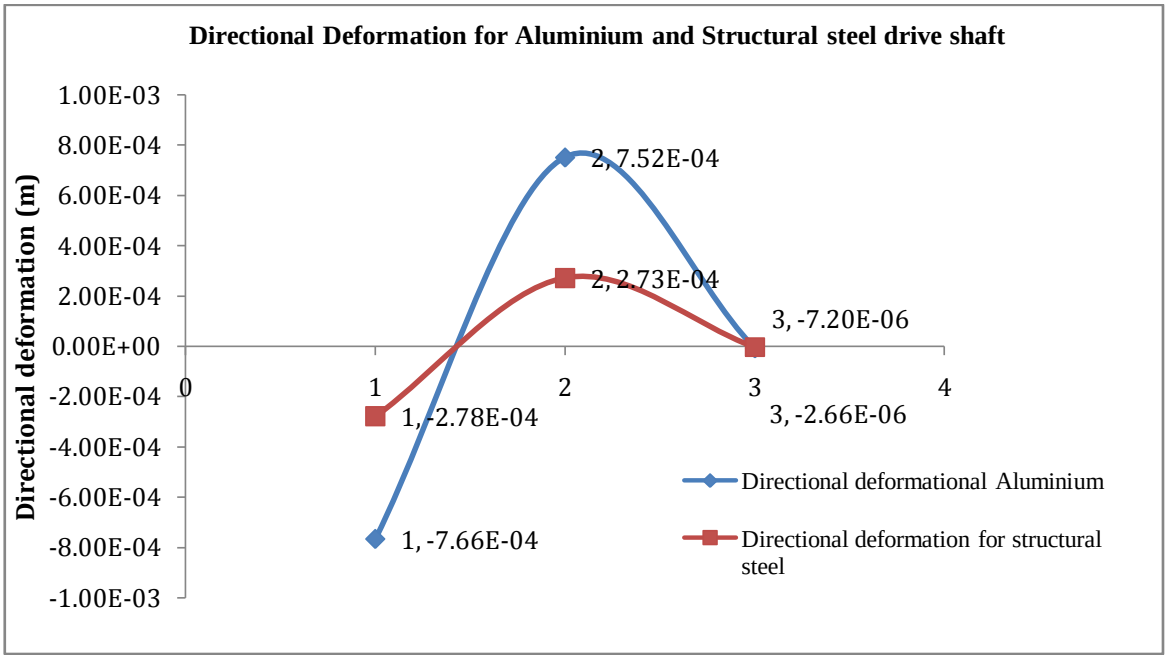

Figure 20: Chart showing directional deformation for aluminium structural steel drive shaft

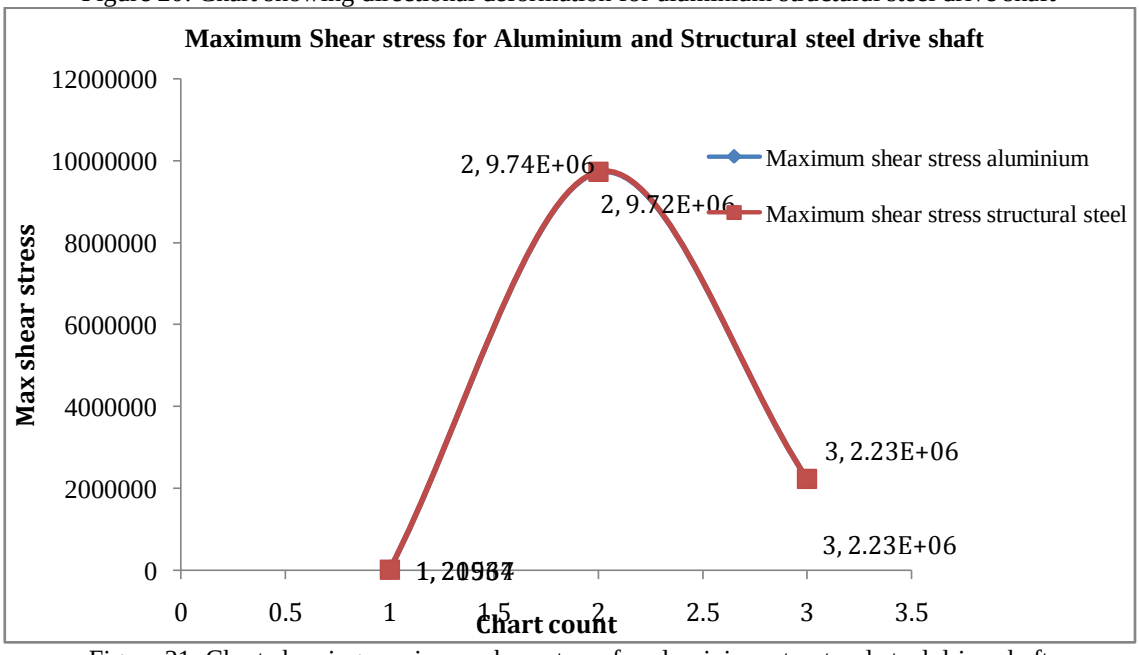

Figure 21: Chart showing maximum shear stress for aluminium structural steel drive shaft

International Journal of Advances in Engineering and Management (IJAEM)
Volume 4, Issue 6 June 2022, pp: 17-39 www.ijaem.net ISSN: 2395-5252

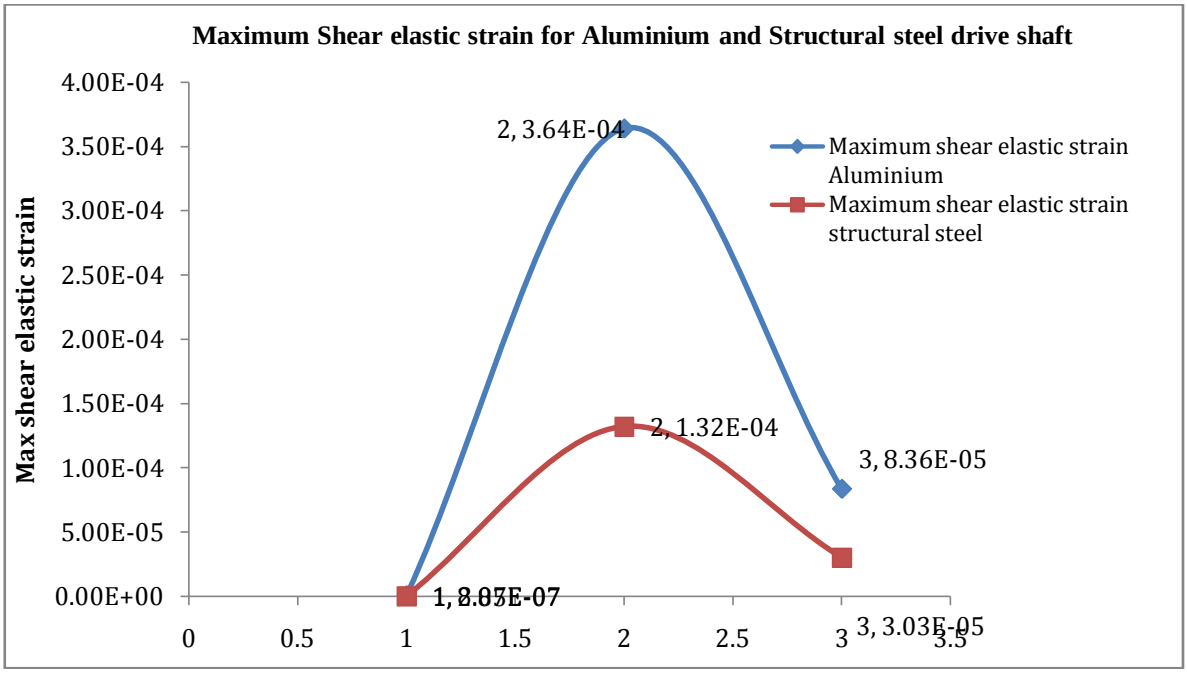

Figure 22: Chart showing maximum shear elastic strain for aluminium structural steel drive shaft

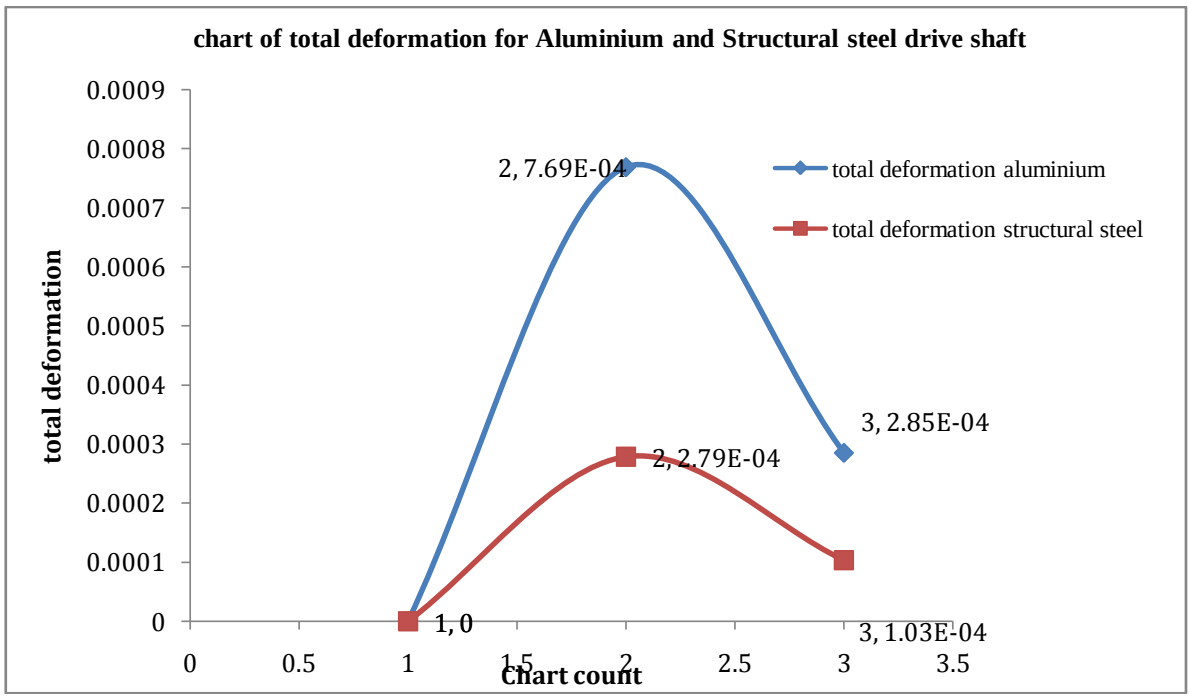

Figure 23: Chart showing total deformation for aluminium structural steel drive shaft

International Journal of Advances in Engineering and Management (IJAEM)
Volume 4, Issue 6 June 2022, pp: 17-39 www.ijaem.net ISSN: 2395-5252

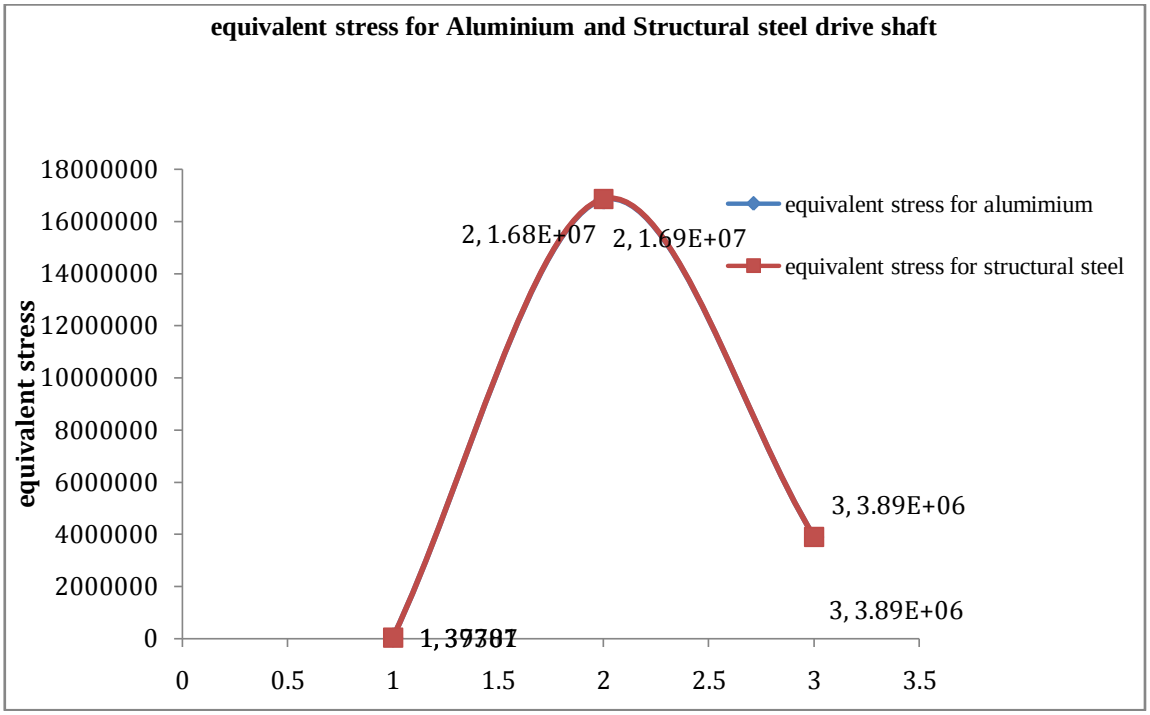

Figure 24: Chart showing equivalent stress for aluminium structural steel drive shaft

Simulation results for the Propeller

The continuum was chosen as fluid and the properties of water were assigned to it. A moving reference frame is assigned to fluid with a rotational velocity (200, 250, 300, 350 and 400rpm).

The maximum pressure exerted by the propellers is seen to be at the intersection of the blade and the surface of the hub. As we look towards the tip of the propeller blade, the pressure decreases, and the pressure is at its lowest in the region surrounding the blade.

CASE 1: The figures 25 and 26 show the pressure distribution and fluid behaviour on and around the propeller at 200 rpm and the gradients also indicate the areas of maximum and minimum pressure on the propeller.

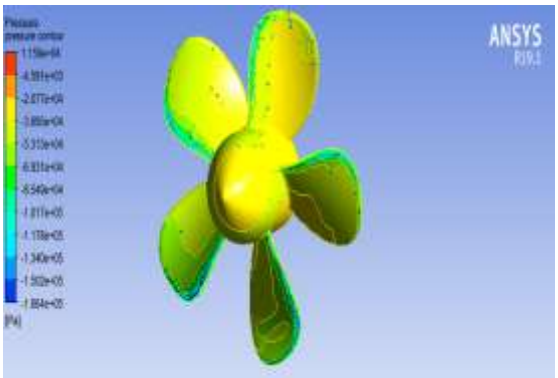

Figure 25: Pressure contour on the propeller at 200 rpm

International Journal of Advances in Engineering and Management (IJAEM)
Volume 4, Issue 6 June 2022, pp: 17-39 www.ijaem.net ISSN: 2395-5252

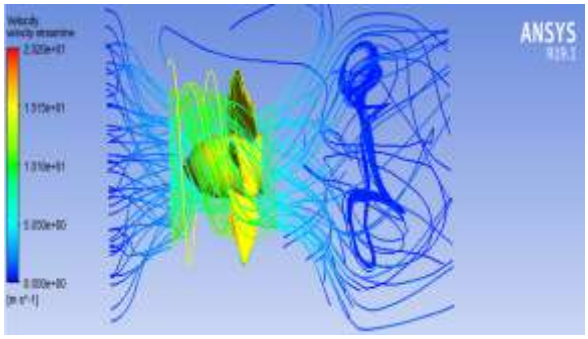

Figure 26: Velocity streamline at 200 rpm

CASE 2: Figures 27 and 28 shows the pressure distribution and fluid behaviour on and around the propeller at 250 rpm and the gradients also indicate the areas of maximum and minimum pressure on the propeller.

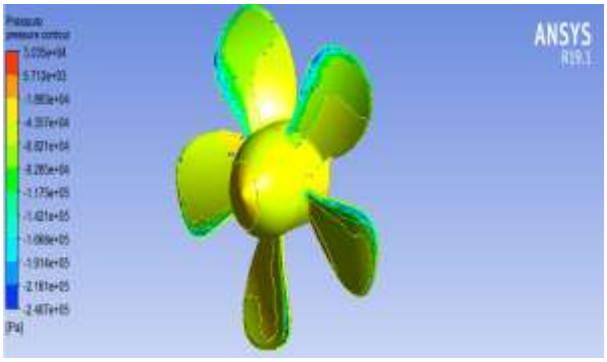

Figure 27: Pressure contour on the propeller at 250 rpm

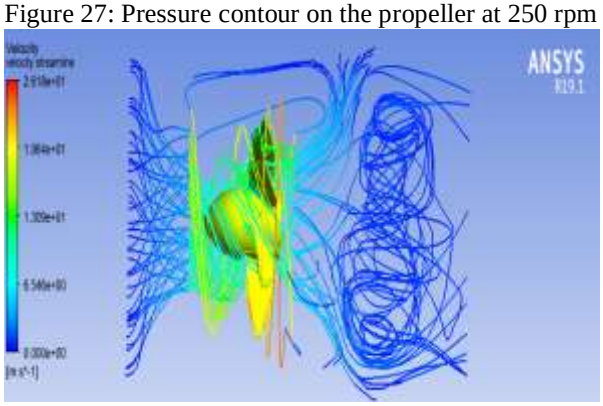

Figure 28: velocity streamline for 250 rpm

CASE 3: Figures 29 and 30 shows the pressure distribution and fluid behaviour on and around the propeller at 300 rpm and the gradients also indicate the areas of maximum and minimum pressure on the propeller.

International Journal of Advances in Engineering and Management (IJAEM)
Volume 4, Issue 6 June 2022, pp: 17-39 www.ijaem.net ISSN: 2395-5252

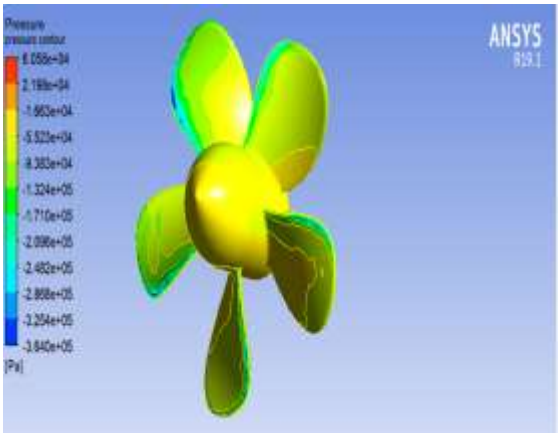

Figure 29: Pressure contour on the propeller at 300 rpm

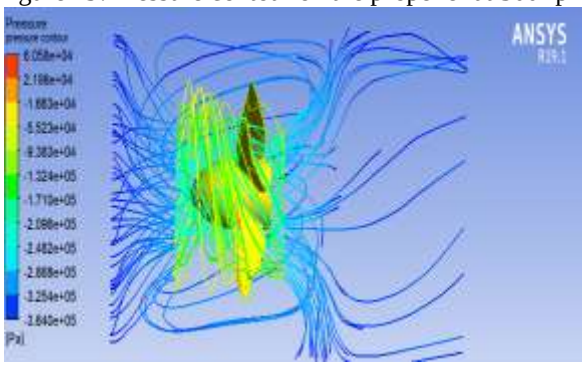

Figure 30: Velocity streamline at 300 rpm

CASE 4: Figures 31 and 32 shows the pressure distribution and fluid behaviour on and around the propeller at 350 rpm and the gradients also indicate the areas of maximum and minimum pressure on the propeller.

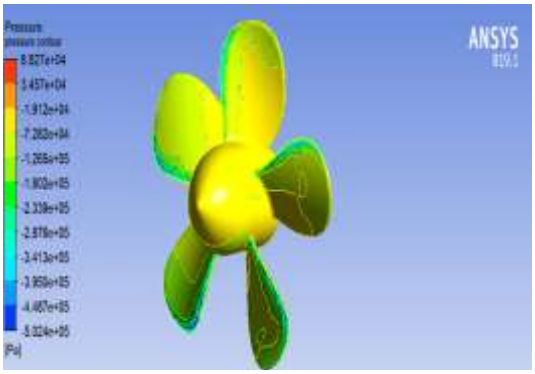

Figure 31: Pressure contour on the propeller at 350 rpm

International Journal of Advances in Engineering and Management (IJAEM)
Volume 4, Issue 6 June 2022, pp: 17-39 www.ijaem.net ISSN: 2395-5252

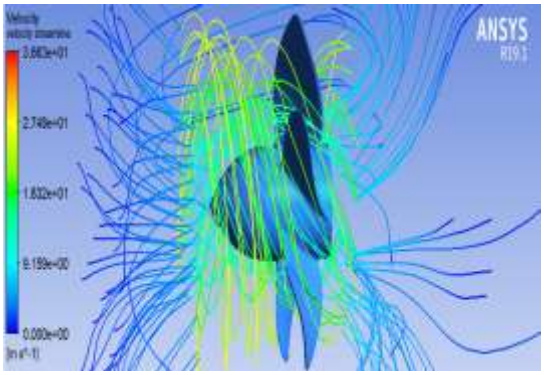

Figure 32: Velocity streamlines 350 rpm

CASE 5: Figures 33 and 34 shows the pressure distribution and fluid behaviour on and around the propeller at 400 rpm and the gradients also indicate the areas of maximum and minimum pressure on the propeller.

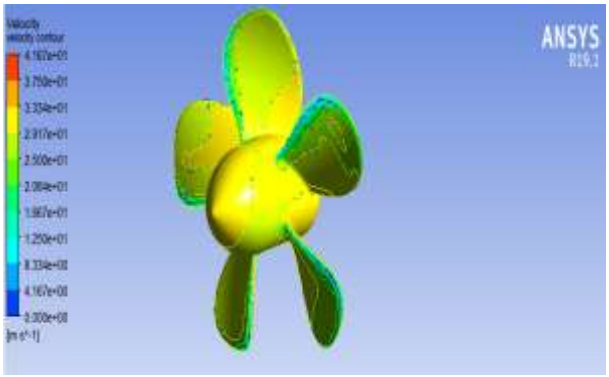

Figure 33: Pressure contour on the propeller at 400rpm

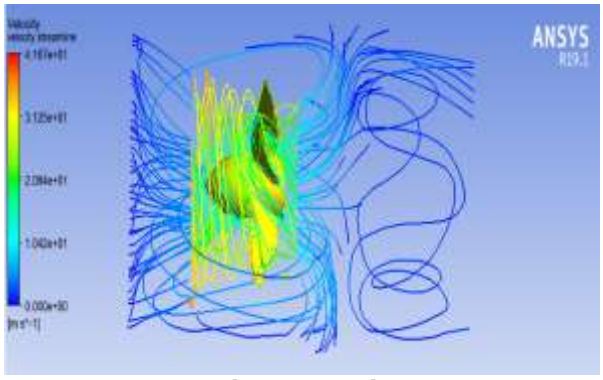

Figure 34: Velocity streamlines 400 rpm

Propeller Thrust Forces

Figure 35 shows that the chart thrust force angle at different rpm ranging from 200 to 400 rpm using each of the different colours as indicated in the figure. The analysis indicates from the chart a steady thrust force output, and as revolution increases the thrust force increases sequentially. At 200rpm, the pressure decreases as the pressure is at its lowest in the region surrounding the blade, and the velocity streamline at 250rpm, at 300rpm the pressure is normal in the region surrounding the blade, and the velocity streamline at 350rpm and at 400rpm the pressure is at its highest in the region surrounding the blade.

International Journal of Advances in Engineering and Management (IJAEM)
Volume 4, Issue 6 June 2022, pp: 17-39 www.ijaem.net ISSN: 2395-5252

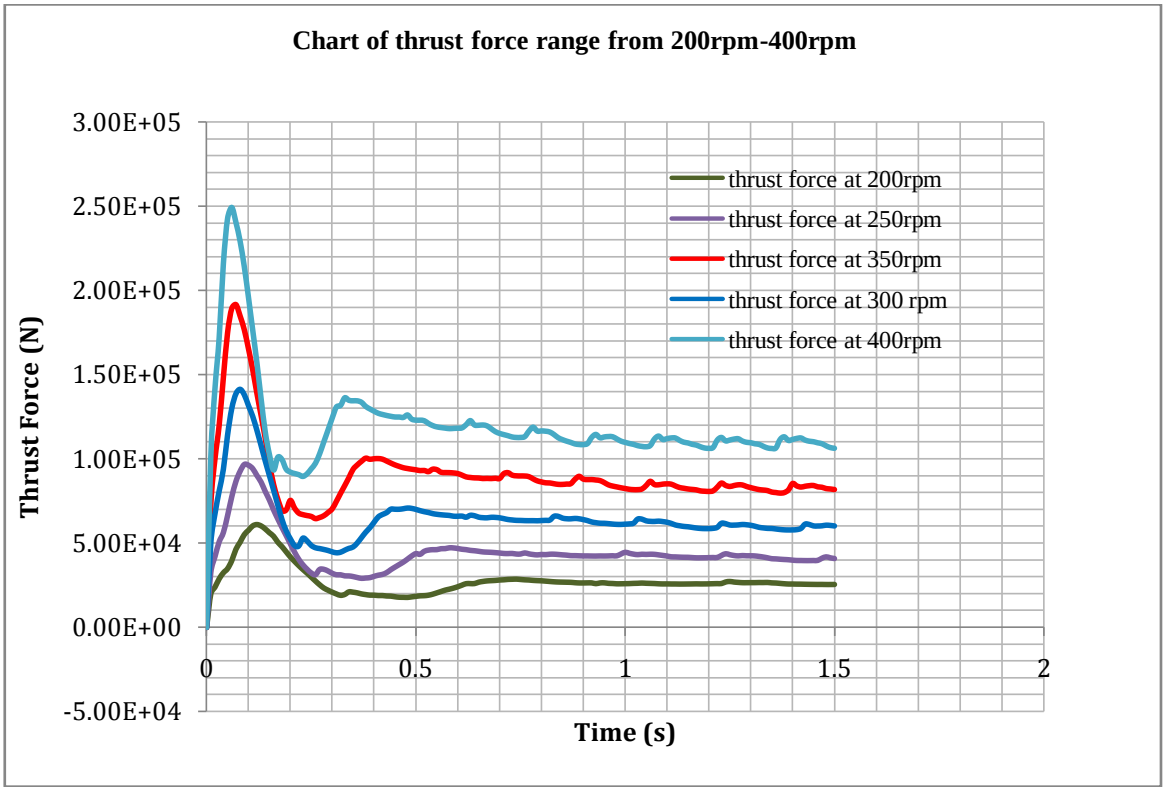

Figure 35:The thrust force angle at different rpm ranging from 200 to 400 rpm using each of the different colours

IV CONCLUSION

The comparative analysis of the propulsion system of a tug boat for optimal performance using aluminium or steel materials has shown that Steel proves to withstand more pressure in the Engine other than that of the aluminium. On the piston of the Main Engine, the materials used for the analyses were aluminium, steel and grey cast iron. These analyses were carried out to determine the total deformation condition of each material at a pressure of 6.289bar at the top of the piston and average cycle pressure of 80bar and steel is observed to be a better material for the piston in terms of both deformation and stress. Graphs were used to explain the analysis. For shafting line, discussions were made on how the reduction gear gives a standard required thrust for the shafting drive line to move the propeller at the efficient torque and revolution. The shafting system analysis were carried out on the materials (aluminium and stainless steel), it was observed that deformation on aluminium is higher than that on the stainless steel at 1800N but the stress distribution on aluminium is lesser to that of the stainless steel. For the propeller, analysis was carried out on the pressure and around the propeller with the rotation velocity from 200rpm-400rpm. Gradient are used to show the pressure distribution, fluid behaviour around the propeller and also indicates the maximum and minimum pressure on the propeller. It was observed that at 350rpm the pressure distribution is minimal to others velocity rotation and the thrust force at 400rpm gives the maximum thrust force and steady time line. So aluminium is not a better material for the design and construction of marine propulsion system in a tug boat.

REFERENCES

[1]. Nitonye, S., Adumene, S. and Howells, U.U. (2017) Numerical Design and Performance Analysis of a Tug Boat Propulsion System, Journal of Power and Energy Engineering, 5, 11, 80-98,doi.org/10.4236/jpee.2017.511007http://www.scirp.org/journal/jpee

[2]. Tamunodukobipi Daniel, Faango Ibelema, Nitonye Samson, Ogbonnaya Ezenwa (2017), Design, Fabrication and Rotodynamic Performance Analysis of Airboat Propulsion System for application in Amphibious Planning Crafts. Nigerian Oil and Gas Industry Content (NOGIC)

Research and Development **Journal**, Vol. 1, No1, 41-48. www.ncdmb.gov.ng

[3]. Puşcaşu A.M, LupescuO, and Bădănac A. Study regarding the structural response of standardcylindrical roller bearings using ANSYS and MESYS p 05012

[4]. Ganesh V, Pradeep K, Srinivasulu K, (2014),Modelling and Analysis of Propeller Blade for its Strength, International Journal of Engineering Research & Technology (IJERT)Vol. 3 Issue 2.

[5]. Nitonye, S. (2017) Numerical Analysis for the Design of the Fuel System of a Sea Going Tug Boat in the Niger Delta. World Journal of Engineering Research and Technology, 3, 161-177. http://www.wjert.org

[6]. Picket L.M., Siebers D.L., (2005), Journal of Engineering for Gas Turbines and Power, 127:187-196

[7]. Liu Z and Karim G.A, (1995) The ignition delay period in dual fuel engines SAE Paper 950466

[8]. Akshat Srivastav, "Design and analysis of piston for 4- stroke bike engine"

[9]. Aksu, S. and Turan, O. (2006) Reliability and Availability of Pod Propulsion Systems Quality. Reliability Engineering International, 22, 41-58. https://doi.org/10.1002/qre.747

[10]. Goering, and Hansen, (2004) Engine and Tractor Power 4th Edition

[11]. Mahdi Hamzehei, Manochehr Rashidi, "Determination of Piston and Cylinder Head Temperature Distribution in a 4- Cylinder Gasoline Engine at Actual Process"

[12]. Wilbur C.T, and Wight D.A,(1992), "Pounder's Marine Diesel Engines", 6th Edition, Butterworth and Heinemann

[13]. Djahida Boucetta and Omar Imine,(2016), Numerical Simulation of the Flow around Marine Propeller Series, Journal of Physical Science and Application 6 (3) 55-61

[14]. Li, Z., Yan, X., Yuan, C., Zhao, J. and Peng, Z. (2011) Fault Detection and Diagnosis of a Gearbox in Marine Propulsion Systems Using Bi-spectrum Analysis and Artificial Neural Networks. Journal of Marine Science Application, 10, 17-24. https://doi.org/10.1007/s11804-011-1036-7

[15]. Woud H.K, Stapersma D,(2003). "Design of Propulsion and Electric Power Generation Systems", IMarEST, ISBN: 1-902536-47-9

[16]. Tran, V.T., Nguyen, H.V., Ma, A.T., Doan, M.T. and Vo, T.C. (2016) Assessment of Marine Propulsion System Reliability Based on Fault Tree Analysis. International Journal of Transportation Engineering and Technology, 2, 55-61.

[17]. Nitonye, S., & Adumene S. (2014). Numerical and experimental analysis for the stability of a 2500 tonnes Offshore Work Boat. International Journal of Applied Science and Engineering, 3 (6), 1041-1053. (http://www.ijaser.com)

[18]. Kades R.D, (1975)"The Design of Propellers for a U.S. Coast Guard Icebraker Tugboat" David W. Taylor Naval Ship Research and Development Centre. USA

[19]. Dick, I. F., & Nitonye, S. (2015). Effect of fluid density on ship hull resistance and powering. International Journal of Engineering Research and General Science, 3 (1), 615-630. (http://www.ijergs.org)

[20]. Okim Bartholomew Ogar, Samson Nitonye and Ikue John-Hope, (2018) Design Analysis and Optimal Matching of a Controllable Pitch Propeller to the Hull and Diesel Engine of a CODOG system, Journal of Power and Energy Engineering, 6, 3, 53-74. https://doi.org/10.4236/jpee.2018.63005 http://www.scirp.org/journal/jpee

[21]. Dong, C., Yuan, C., Liu, Z. and Yan, X. (2013) Marine Propulsion System Reliability Research Based on Fault Tree Analysis. Advanced Shipping and Ocean Engineering, 2, 27-33.

[22]. Mohammed Ahmed Khan, Khaja Shahnawaz Uddin, Bilal Ahmed,(2013), Design And Dynamic Analysis on Composite Propeller of Ship Using Fea, International Journal of Advanced Trends in Computer Science and Engineering, Vol.2 , No.1, Pages : 310 - 315

[23]. Seetharama R,Rao, and Mallikarjuna Rao K, Sridhar B Reddy, (2012), Stress Analysis of Composite Propeller by Using Finite Element Analysis, International Journal of Engineering Science and Technology (IJEST), Vol. 4 No.08

[24]. Palle Prasad, and Lanka Bosu Babu, (2017), Design And Analysis of the Propeller Blade, International Journal Of Advances In Mechanical And Civil Engineering, Volume-4,Issue-2

[25]. Abhijeet H. Kekan & P.S Kachare, (2012), Static and Dynamic Analysis of Composite Ship Propeller Using FEA, International Conference on Mechanical and Industrial Engineering (ICMIE), Pune.

[26]. American Bureau of Shipping (ABS) (2019) Guidance Notes on Propulsion Shafting

Alignment. American Bureau of Shipping, Houston.
[27]. Lewis, V. and Edward, Ed. (1989) Principle of Naval Architecture, Society of Naval Architects and Marine Engineers.
[28]. Eastop T.D, and McConkey A(1994), "Applied Thermodynamics", Longman Scientific and Technical, ISBN: 0-582-09193-4
[29]. Archer S,(1976). "Some Factors Influencing the Life of Marine Crankshafts", Trans. IME, pp. 73-134
[30]. Ashraf, K.N. (2017) Identification of the Actual Distribution of Demand for Spare Parts in Car Maintenance Service Stations. American Journal of Traffic and Transportation Engineering, 2, 26-31.
[31]. Hongxia, P. and Liming, S. (2012) System Modelling and Application in Gearbox Fault Diagnosis Based on EMD and ARX Model. Applied Mechanics and Materials, 109, 532-536. https://doi.org/10.4028/www.scientific.net/AMM.109.532
[32]. Onwuegbuchunam, D.E., Ogwude, I.C., Igboanusi, C.C., Okeke, K.O. and Azian, N.N. (2020) Propulsion Shaft and Gearbox Failure in Marine Vessels: A Duration Model Analysis. Journal of Transportation Technologies, 10, 291-305. https://doi.org/10.4236/jtts.2020.104019
[33]. Yue, Y. and Zhu, C. (2014) The Application and Research of Order Analysis in Gearbox Fault Diagnosis. Applied Mechanics and Materials, 635-637, 844-850. https://doi.org/10.4028/www.scientific.net/AMM.635-637.844
[34]. Zhang, Y. (2006) Order Bi-spectrum Based Gearbox Fault Diagnosis during Speed-Up Process. Proceedings of the 6th World Congress on Intelligent Control and Automation, Dalian, 21-23 June 2006, 5526.
[35]. Nitonye, S., and Ofanson U (2018) Analysis of Marine Pollution of Ports and Jetties in Rivers State, Nigeria, Open Journal of Marine Science, 8, 1, 114-135. https://doi.org/10.4236/ojms.2018.81006 http://www.scirp.org/journal/ojms